

ARTICLE TYPE**Further evidences of superluminal AGNs as γ -ray sources**Hubing Xiao^{1,2,3} | Junhui Fan^{*1,4,6} | Riccardo Rando^{2,3} | Jingtian Zhu¹ | Liangjun Hu⁵¹Center for Astrophysics, Guangzhou University, Guangzhou, 510006, China²Department of Physics and Astronomy "G. Galilei", University of Padova, Padova PD, 35131, Italy³INFN, University of Padova, Padova PD, 35131, Italy⁴Astronomy Science and Technology Research Laboratory of Department of Education of Guangdong Province, Guangzhou University, Guangzhou, 510006, China⁵School of physics and electronic information, Anhui normal University, Wuhu, 241000, China⁶Key Laboratory for Astronomical Observation and Technology of Guangzhou, Guangzhou University, Guangzhou, 510006, China**Correspondence**

*Junhui Fan, Email: fjh@gzhu.edu.cn

Funding Information

National Natural Science Foundation of China, NSFC 11733001 and NSFC U1531245. Natural Science Foundation of Guangdong Province, 2019B030302001. 2017A030313011. Science and Technology Program of Guangzhou, 201707010401.

In our previous work in Xiao et al. (2019), we suggested that 6 superluminal sources could be γ -ray candidates, and in fact 5 of them have been confirmed in the fourth *Fermi*-LAT source catalogue (4FGL). In this work, based on the 4FGL, we report a sample of 229 *Fermi* detected superluminal sources (FDSs) including 40 new FDSs and 62 non-*Fermi* detected superluminal sources (non-FDSs). Thus, we believe that all superluminal sources should have γ -ray emissions, and superluminal motion could also be a clue to detect γ -ray emission from active galactic nuclei (AGN). We present a new approach of Doppler factor estimate through the study of the γ -ray luminosity (L_γ) and of the viewing angle (ϕ).

KEYWORDS:active galactic nuclei, jets, γ -rays, superluminal motion, 4FGL**1 | INTRODUCTION**

Active galactic nuclei (AGNs) are a hot topic in astrophysics since they were discovered in the 1960s, while their nature is still object of investigation. Blazars, a very extreme subclass of AGNs, show rapid and high variability, high and variable polarization, variable and strong γ -ray emission and even superluminal motions (von Montigny et al. 1995; Fan et al. 2013a; Fan et al. 2013b; Xiao et al. 2019). These extreme

observational properties of blazars are mainly due to the presence of a relativistic jet (Blandford & Königl. et al. 1979). Blazars have two subclasses, namely BL Lacertae objects (BL Lacs) and flat spectrum radio quasars (FSRQs). Spectra of BL Lacs show weak or no emission lines while FSRQs show strong emission line features.

Fermi-LAT (*Fermi* Large Area Gamma-Ray Space Telescope), which was launched 2008, provides us with good opportunities to detect GeV γ -ray sources, for instance blazars. The third *Fermi*-LAT source catalogue (3FGL), which draws up a list of the first 4 years data, contains 3034 γ -ray sources,

out of them 1459 are blazars. The *Fermi* detected blazar sample is enlarged by the fourth *Fermi*-LAT source catalogue (4FGL), which concludes with 2938 blazars out of 5098 γ -ray sources from 8 years data (*Fermi* LAT collaboration. 2019). The γ -ray detections of blazars can be used to investigate the emission mechanism of the high energetic γ -ray emissions. The correlations between γ -ray luminosity and other band luminosities (radio, optical, and X-ray emissions) were discussed by many authors in literature (Dondi & Ghisellini 1995; Fossati et al. 1998; Fan et al. 2016; Zhang & Fan 2018). It was found that the correlation between γ -ray and radio emission is the result of a self-synchrotron Compton (SSC) emission. The evidence that the γ -ray emission in blazars is strong also suggests the existence of a relativistic beaming effect (Arshakian et al. 2010; Fan et al. 2013a; Fan et al. 2013b; Fan et al. 2017; Giovannini et al. 2014; Giroletti et al. 2012; Kovalev et al. 2009; Massaro et al. 2013a; Massaro et al. 2013b; Savolainen et al. 2010; Xiao et al. 2015; Pei et al. 2016; Yang et al. 2017; Yang et al. 2018a; Zhang & Fan 2018; Xiao et al. 2019).

An interesting observational phenomenon in blazars is the presence of superluminal motions (sources with apparent velocity larger than the speed of light, $\beta_{\text{app}} > 1$), which is also a consequence of the beaming effect. In 1996, Fan et al. compiled a sample of 48 superluminal sources in order to investigate the beaming effect and found that the core dominance parameter, the ratio of core radio flux to the extended radio flux, is an indicator of the orientation of the emission. They proposed that the superluminal motion and beaming effect are probably two aspects of the same phenomenon. Zhang & Fan (2008) collected a sample of 123 superluminal sources and found that the radio emissions are strongly boosted by the beaming effect and that the superluminal motion is another indicator of the beaming effect in AGNs. Lister et al. (2009) found that there is an overwhelming tendency to display outward motions, studying the radio flux of 135 radio-loud AGNs extracted from the MOJAVE¹ (Monitoring of Jets in Active galactic nuclei with VLBA Experiments) sample. Lister et al. (2013) studied jet orientation variations and superluminal motions of 200 AGNs and found a general trend of increasing apparent speed with increasing distance along the jet for both radio galaxies and BL Lac objects. In Xiao et al. (2019), we collected 291 superluminal sources, including 189 FDSs (*Fermi* Detected γ -ray Superluminal sources) and 102 non-FDSs (non-*Fermi* Detected Superluminal sources) to study the difference between FDSs and non-FDSs. We found that FDSs are more strongly beamed than non-FDSs, and we claimed that some superluminal sources are γ -ray emission candidates. This suggestion is further confirmed by the data of the 4FGL release

(*Fermi* LAT collaboration. 2019), which allow to extend our previous study.

This work is arranged as follows: In section 1, we introduce the background of γ -ray blazars and of the superluminal motion; in section 2, we give our sample and results; discussion and conclusions are presented in sections 3 and 4.

2 | SAMPLES AND RESULTS

2.1 | Samples

In Xiao et al. (2019), we identified, in the 3FGL catalogue, 291 superluminal sources, out of them which 189 FDSs and 102 non-FDSs.

We matched the sources in our non-FDSs sample with the sources in the 4FGL catalogue and found that 40 of 102 sources that were non-FDSs in 3FGL are FDSs in 4FGL. They are listed in Table 1. Hence, we have an updated sample of 229 FDSs from 3FGL and 4FGL, and remain 62 non-FDSs.

Meanwhile, the corresponding source information, optical magnitude, radio flux, X-ray flux density, 3FGL γ -ray flux density, from Xiao et al. (2019) will be also employed in this work. In Table 1, we only listed the 40 new FDSs, column (1) the source 4FGL name; column (2) other name; column (3) classification, F = FSRQs, B = BL Lacs, Sy = Seyfert galaxy, G = galaxy and U = BCU, (blazar candidates of uncertain type) through this paper; column (4) redshift; column (5) and (6) radio Doppler factor and its corresponding reference, H09 is Hovatta et al. (2009), L18 means Lioudakis et al. (2018); column (7), (8) and (9) are the integral photon flux and uncertainty from 1 to 100 GeV and its photon index from 4FGL.

2.2 | Results: Correlation between γ -ray band luminosity and other band luminosities for FDSs

We studied the correlations between γ -ray luminosity and luminosity in other wavelength ranges (radio, optical, X-ray) for the FDSs. The multi-wavelength (radio, optical and X-ray) data are collected from the BZCAT, the γ -ray photon flux ($\text{photons}/\text{s}/\text{cm}^2$) are collected from 3FGL and 4FGL. The optical magnitude has been corrected by Galactic extinction correction and transformed to flux density. Then, the radio, optical, X-ray and γ -ray flux densities has been all multiply by $(1+z)^{\alpha-1}$ in order to introduce the K -correction. For the spectral indices (α), we adopt $\alpha_r = 0$ in the radio band (Donato et al. 2001, Abdo et al. 2010), and in the X-ray band $\alpha_x = 0.78$ for FSRQs, $\alpha_x = 1.30$ for BLs and $\alpha_x = 1.05$ for BCUs (blazar candidates of uncertain type) as suggested by Fan et al. (2016).

¹<http://www.physics.purdue.edu/MOJAVE/>

TABLE 1 New FDSs from 4FGL.

4FGL name	Other name	Class	redshift	δ_R	Ref.	Flux1000 <i>photons/cm²/s</i>	Flux1000_error <i>photons/cm²/s</i>	α_{ph}
(1)	(2)	(3)	(4)	(5)	(6)	(7)	(8)	(9)
4FGL J0006.3-0620	0003-066	B	0.347	6.96	L18	1.26E-10	3.35E-11	2.1704
4FGL J0013.6+4051	0010+405	F	0.255	8.81	L18	1.81E-10	3.52E-11	2.212
4FGL J0019.6+7327	0016+731	F	1.781	7.84	L18	1.27E-09	7.91E-11	2.5943
4FGL J0037.6+3653	0035+367	F	0.366			1.67E-10	3.63E-11	2.3478
4FGL J0109.7+6133	0106+612	G	0.783	23.74	L18	2.56E-09	1.15E-10	2.6068
4FGL J0112.0+3442	0109+351	F	0.45	1.57	L18	1.51E-10	3.34E-11	2.3388
4FGL J0115.1-0129	0112-017	F	1.365	14.55	L18	2.44E-10	4.02E-11	2.7209
4FGL J0125.7-0015	0122-003	F	1.074	20	L18	1.22E-10	3.01E-11	3.0257
4FGL J0152.2+2206	0149+218	F	1.32	4.32	L18	3.75E-10	4.65E-11	2.7059
4FGL J0210.7-5101	0208?512	F	1.003			4.19E-09	1.09E-10	2.3536
4FGL J0228.7+6718	0224+671	F	0.53	6.01	L18	5.05E-10	6.64E-11	2.545
4FGL J0231.8+1322	0229+131	F	2.059	11.31	L18	4.48E-10	5.26E-11	2.7412
4FGL J0359.6+5057	0355+508	F	1.52	6.12	L18	2.29E-09	1.29E-10	2.6416
4FGL J0403.3+2601	0400+258	F	2.109	7.59	L18	2.32E-10	4.63E-11	2.6
4FGL J0433.0+0522	0430+052	F	0.033	1.09	L18	6.94E-10	7.56E-11	2.7163
4FGL J0539.6+1432	0536+145	F	2.69	22.59	L18	8.14E-10	7.78E-11	2.5573
4FGL J0555.6+3947	0552+398	F	2.365	25.2	H09	6.63E-10	7.13E-11	2.8018
4FGL J0728.0+6735	0723+679	Sy1.2	0.846			1.08E-10	2.60E-11	3.0044
4FGL J0746.0-0039	0743-006	F	0.994	4.7	L18	1.42E-10	3.91E-11	2.629
4FGL J0748.6+2400	0745+241	F	0.409	1.81	L18	6.74E-10	5.59E-11	2.2817
4FGL J0808.5+4950	0804+499	F	1.435	8.63	L18	2.26E-10	3.38E-11	2.8056
4FGL J0836.5-2026	0834-201	F	2.752			1.81E-10	4.88E-11	2.8311
4FGL J0850.0+5108	0846+513	F	0.585	22.77	L18	2.16E-09	7.90E-11	2.2701
4FGL J0910.0+4257	0906+430	F	0.67			2.41E-10	3.61E-11	2.5156
4FGL J0958.0+4728	0955+476	F	1.882	12.01	L18	3.87E-10	4.22E-11	2.6414
4FGL J1037.4-2933	1034-293	F	0.312	2.8	F09	3.58E-10	4.79E-11	2.4824
4FGL J1051.6+2109	1049+215	F	1.3	6.29	L18	1.68E-10	3.51E-11	2.7773
4FGL J1131.0+3815	1128+385	F	1.74			7.83E-10	6.03E-11	2.5512
4FGL J1131.4-0504	1128-047	G	0.266	0.51	L18	3.11E-10	5.72E-11	2.4798
4FGL J1159.3-2142	1157-215	F	0.927			1.17E-09	7.37E-11	2.5131
4FGL J1459.0+7140	1458+718	Sy 1.5	0.905	3.92	L18	2.14E-10	2.84E-11	2.4462
4FGL J1534.8+0131	1532+016	F	1.42	10.13	L18	1.03E-09	6.79E-11	2.3663
4FGL J1638.1+5721	1637+574	F	0.75	7.97	L18	2.98E-10	3.25E-11	2.6426
4FGL J1753.7+2847	1751+288	F	1.115	3.81	L18	1.68E-10	3.70E-11	2.3828
4FGL J2011.6-1546	2008-159	F	1.18	7.75	L18	1.96E-10	4.84E-11	2.841
4FGL J2038.7+5117	2037+511	F	1.686	19.86	L18	1.28E-09	1.21E-10	2.616
4FGL J2123.6+0535	2121+053	F	1.941	10.31	L18	4.33E-10	5.15E-11	2.3652
4FGL J2219.2-0342	2216-038	F	0.901	12.23	L18	1.74E-10	4.04E-11	2.8928
4FGL J2225.6+2120	2223+210	F	1.959	11.26	L18	2.05E-10	3.81E-11	2.8114
4FGL J2354.6+4554	2351+456	F	1.992	3.36	L18	2.22E-10	4.11E-11	2.4002

Considering that the luminosity is correlated with the redshift, we have removed its influence in order to achieve the pure correlation of the luminosities through a partial correlation analysis:

$$r_{ij,k} = \frac{r_{ij} - r_{ik}r_{jk}}{\sqrt{(1 - r_{ik}^2)(1 - r_{jk}^2)}}$$

here r_{ij} , r_{ik} , r_{jk} are the correlation coefficients between any pair of variables i , j and k . In this work, the variables i and j represent luminosities of two bands, the variable k represents redshift.

Any study of blazar radiation must take into account the presence of Doppler beaming effect, in order to identify correlations between luminosities in different spectral bands. The correlation between observed (beamed) flux, f^{ob} , and intrinsic (de-beamed) flux, f^{in} , is $f^{\text{in}} = f^{\text{ob}}/\delta^p$, where, δ is the Doppler factor, and $p = 2 + \alpha$ for continuous flow, $p = 3 + \alpha$ for discrete flow, respectively. The correlation between observed (beamed) luminosity and intrinsic (de-beamed) luminosity is $L^{\text{in}} = L^{\text{ob}}/\delta^{1+p}$. The optical, δ_o , and the X-ray, δ_x , Doppler factors, were derived from the radio Doppler factor, δ_r , through an empirical method proposed by Fan et al. (1993): $\delta_o = \delta_o^{1+1/8 \log(v_o/v)}$, where δ_o is the optical Doppler factor, and $\delta_x \sim \delta_o^{0.5}$, $\delta_r \sim \delta_o^{1.5}$ are corresponding factors of the X-ray and radio ranges respectively. The γ -ray Doppler factor is the same as the radio Doppler factor, because the radio and γ -ray emission arise from the same region in a leptonic model.

Figure 1 reports the distribution of pairs of observed beamed luminosities (left column) and the distribution of pairs of corresponding de-beamed luminosities (right column). The dots in the encircled regions have been excluded from the evaluation of the best fit of the distributions on the base of considerations reported in section 3.2. Table 2 quotes the following parameters: a and b are slope and intercept of the linear best fit; Δa and Δb are the corresponding uncertainties; N is the total number of sources, the number in parentheses represents the number of sources we neglected in the regression; r and p are the correlation coefficient and the chance probability, respectively.

3 | DISCUSSION

3.1 | New sources

In our previous work in Xiao et al. (2019), we predicted 6 non-FDS sources to be γ -ray candidates, 0153+744, 0208-512, 0536+145, 0552+398, 2223+210, 2351+456, with a criterion that $\beta_{\text{non-FDS}}^{\text{max}} > \langle \beta_{\text{FDS}}^{\text{max}} \rangle + 5\sigma$ (Xiao et al. 2019). Out of these 6 candidates, 5 sources have been identified through 4FGL as 4FGL J0210.7-5101 (0208-512), 4FGL J0539.6+1432 (0536+145), 4FGL J0555.6+3947 (0552+398), 4FGL J2225.6+2120 (2223+210) and 4FGL J2354.6+4554 (2351+456).

In addition, we found 40 non-FDS sources from Xiao et al. (2019) as new FDS sources in 4FGL. Thus, for 291 available superluminal sources, 229 are Fermi-detected sources, namely 78.7 % of the superluminal sources, while the remaining 62

(21.3%) have no available Fermi detection. We suspect that all these non-FDS sources quite likely have a faint γ -ray emission, which lays under the level of the detectability of *Fermi*-LAT.

3.2 | Correlations

Correlations between the γ -ray luminosity and their corresponding luminosity in the radio, optical and X-ray bands for FDS sources are shown in Figure 1. Their numerical features are listed in Table 2. The left panel, Figure 1 a, c, e, shows the correlations of $\log L_\gamma$ vs $\log L_{r, o, x}$, where the luminosities are boosted by Doppler beaming effect. Meanwhile, the right panel, Figure 1 b, d, f, shows the correlations of the de-beamed luminosities.

Six sources, (1) 3FGL J0205.0+1510 (4C +15.05), (2) 3FGL J0325.2+3410, (3) 4FGL J0433.0+0522, (4) 3FGL J0710.5+4732 (S4 0707+47), (5) 3FGL J1104.4+3812 (Mrk 421), and (6) 3FGL J1517.6-2422 (AP Lib) were removed before calculating the linear regression. In the subplot (a), only one source, Mrk 421 was removed. This source is a typical high synchrotron peak frequency source (HSP) and shows relatively lower radio band luminosity. In subplot (c), 5 sources are circled. Source 1 has low optical luminosity. Source 4 has both high observed and high intrinsic luminosity in subplots (c) and (d). Sources 2, 3, 6 have relatively low L_γ , among them sources 2 and 3 are both Seyfert galaxies, and source 6 is a BL Lac object. In subplot (e), only source 3 is neglected. We did not circle any points in subplot (f), since the scatters are relatively well distributed separately in this subplot.

In Figure 1 a, c, e, where the beaming effect is still present the correlation coefficients: 0.14, 0.25 and 0.33 indicate weak correlation of luminosities. The same coefficients become 0.87, 0.82, 0.75 respectively after corrections of beaming effect, namely dividing the luminosities by δ^{1+p} , see Figure 1 b, d, f.

Therefore, the beamed observed luminosities show weak correlation, whereas the de-beamed intrinsic luminosities show strong correlation. A result which suggests that the radio, optical and X-ray emissions are all beamed.

3.3 | γ -ray Luminosity and Viewing Angle

Considering the presence of a strong beaming effect in these superluminal sources, especially FDSs, we expected some good correlation between γ -ray Luminosity (L_γ) and Viewing Angle (ϕ). Therefore, we collected 181 FDSs with available Doppler factor from literature (δ_{Ref}) and maximum apparent velocity of all components, which are the individual bright features apart from the core region, from Xiao et al. (2019). These data are listed in Table 3, where we give: column (1) name; column (2) other name; column (3) classification; column (4)

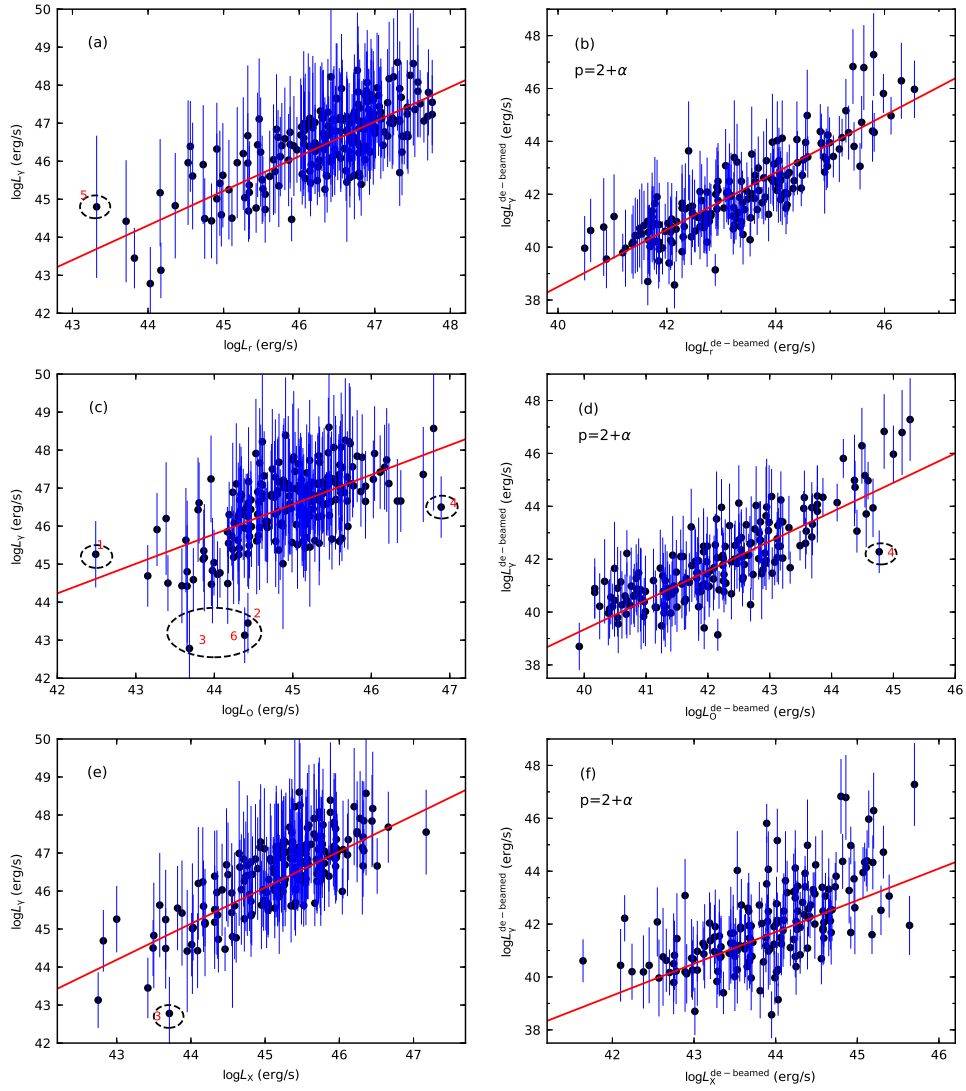


FIGURE 1 Plots for γ -ray band and other bands luminosity correlations for FDS. Left-hand panel for beamed results, right-hand panel for de-beamed results. Upper panel for γ -ray band against radio band, middle panel for γ -ray against optical and lower panel for γ -ray against X-ray band. Black dots with blue error-bar, calculated from the corresponding uncertainties that collected from 3FGL and 4FGL, for the FDS sources, and the red solid lines stand for best linear fitting results.

redshift; column (5) Doppler factor, δ_{Ref} ; column (6) reference for δ_{Ref} ; column (7) 3FGL integral photon flux from 1 to 100 GeV; column (8) γ -ray photon spectral index; column (9) maximum apparent velocity; column (10) estimated Doppler factor of this work, $\delta_{\text{TW}}^{L_\gamma}$.

We found a significant anti-correlation, see Figure 2 a, between observed γ -ray luminosity (L_γ) and viewing angle

(ϕ),

$$\phi = -(2.63 \pm 0.31) \log L_\gamma^{\text{ob}} + (127.02 \pm 14.48),$$

with $r = -0.54$ and $p = 1.1 \times 10^{-14}$.

While, there is a positive correlation between intrinsic γ -ray luminosity (L_γ^{in} , which can be determined with $L_\gamma^{\text{in}} = L_\gamma^{\text{ob}} / \delta^{1+p}$) and viewing angle (ϕ),

$$\phi = (1.81 \pm 0.20) \log L_\gamma^{\text{in}} + (-71.20 \pm 8.28), \quad (p = 2 + \alpha)$$

TABLE 2 γ -ray flux luminosity *vs* other bands luminosities partial correlation analysis results.

Type	band	Type	$a + \Delta a$	$b + \Delta b$	N	r	p
FDS	$\log L_\gamma$ <i>vs</i> $\log L_r$	beamed	0.91 ± 0.06	4.27 ± 2.65	213+(1)	0.14	4.0%
		de-beamed	1.07 ± 0.05	-4.70 ± 2.09	180	0.87	2.2×10^{-55}
	$\log L_\gamma$ <i>vs</i> $\log L_o$	beamed	0.78 ± 0.07	11.47 ± 3.18	209+(5)	0.25	2.2×10^{-4}
		de-beamed	1.11 ± 0.06	-5.06 ± 2.60	178+(1)	0.82	1.8×10^{-45}
	$\log L_\gamma$ <i>vs</i> $\log L_x$	beamed	0.95 ± 0.06	3.34 ± 2.57	201+(1)	0.33	2.3×10^{-6}
		de-beamed	1.20 ± 0.13	-11.10 ± 5.68	170	0.75	1.3×10^{-31}

TABLE 3 181 FDSs with available Doppler factor.

Fermi name	Other name	Class	redshift	δ_{Ref}	Ref.	Flux1000 <i>photons/cm²/s</i>	α_{ph}	$\beta_{\text{app}}^{\text{max}}$ <i>c</i>	$\delta_{\text{TW}}^{\text{L}\gamma}$
(1)	(2)	(3)	(4)	(5)	(6)	(7)	(8)	(9)	(10)
3FGL J0006.4+3825	S4 0003+38	F	0.229	5.23	L18	6.06E-10	2.62	4.6	1.33
3FGL J0051.0-0649	0048-071	F	1.975	5.61	L18	1.40E-09	2.10	13.4	37.32
3FGL J0102.8+5825	TXS 0059+581	F	0.644	18.51	L18	6.18E-09	2.09	8.62	18.97
3FGL J0108.7+0134	4C+01.02	F	2.099	2.64	L18	5.27E-09	2.26	25.8	69.03
3FGL J0112.8+3207	0110+318	F	0.603	10.21	L18	3.04E-09	2.36	19	9.91
...

with $r = 0.57$ and $p = 1.3 \times 10^{-16}$.

$$\phi = (1.67 \pm 0.15) \log L_\gamma^{\text{in}} + (-63.19 \pm 6.16), \quad (p = 3 + \alpha)$$

with $r = 0.64$ and $p = 8.8 \times 10^{-22}$. We show the last two correlations in Figure 2 b, c: the circles indicate the sources, and the solid red line represents the best linear regression. Four sources (3FGL J1015.0+4925, 3FGL J1058.6+5627, 3FGL J1510.9-0542, 3FGL J1653.9+3945), which lie within a rectangle in Figure 2 a, b, c have been neglected in the derivation of the linear regressions.

The opposite correlations of $\log L_\gamma$ and ϕ indicate a strong beaming effect. If we hold these two correlations, then an estimate of the Doppler factor can be obtained as of function of γ -ray observed luminosity and the photon index. We use the two correlations as formulas couple with $L_\gamma^{\text{in}} = L_\gamma^{\text{ob}} / \delta^{1+p}$ and $\alpha = \alpha_{\text{ph}} - 1$, to derive a formula, which allows to estimate the Doppler factor:

$$\delta^{\text{L}\gamma} = 10^{\frac{2.45 \log L_\gamma^{\text{ob}} - 109.51}{3 + (\alpha_{\text{ph}} - 1)}}, \quad (p = 2 + \alpha), \text{ and}$$

$$\delta^{\text{L}\gamma} = 10^{\frac{2.57 \log L_\gamma^{\text{ob}} - 113.90}{4 + (\alpha_{\text{ph}} - 1)}}, \quad (p = 3 + \alpha)$$

With this formula, we calculated the Doppler factor for the 181 FDSs, and listed the estimated Doppler factor $\delta_{\text{TW}}^{\text{L}\gamma}$ in the last column in Table 3 . Then the K-S test between δ_{Ref} and $\delta_{\text{TW}}^{\text{L}\gamma}$ for each case, apart from the 4 sources in the rectangle, was applied to distinguish the two distributions. The results are listed in Table 4 , which quotes: column (1) the condition

applied to choose sources from the sample of 181 FDSs; column (2) $p = 2 + \alpha$ and $p = 3 + \alpha$ for the continuous flow and the discrete flow respectively; column (3) classification; column (4) number of sources; columns (5) and (6) report the statistics value and the p-value from the K-S test results. The results corresponding to a *statistics* = 0.07 and *p-value* = 71.0% for the case $p = 3 + \alpha$, in Table 4 and Figure 3 , show that it is reasonable to affirm that the distributions of the two samples are the same.

By using our ‘luminosity-Doppler factor’ formula, we calculated $\delta^{\text{L}\gamma}$ for 4FGL blazars, with available redshift from literature, and listed the results in Table 5 , where we quote: column (1) name; column (2) classification; column (3) redshift; column (4) 4FGL Integral photon flux from 1 to 100 GeV; column (5) 4FGL γ -ray photon spectral index; column (6) estimated luminosity-Doppler factor from this work. This $\delta^{\text{L}\gamma}$ is neither a upper limit nor a lower limit of a real Doppler factor, but we may use it as comparison for further Doppler factor calculations and beaming effect studies.

Meanwhile, we applied both beaming model with $p = 2 + \alpha$ and $p = 3 + \alpha$ valid in the case of continuous flow and discrete flow respectively and found, comparing δ_{ref} with $\delta_{\text{TW}}^{\text{L}\gamma}$,

TABLE 4 K-S test of δ_{Ref} vs $\delta_{\text{TW}}^{L_\gamma}$.

Filter (1)	p (2)	Class (3)	N (4)	statistics (5)	p-value (6)
with $\phi < 30^\circ$ (deduct 4 sources)	$2 + \alpha$	All	177	0.12	15.4 %
		FSRQ	142	0.11	31.0 %
		BL Lac	29	0.24	32.1 %
	$3 + \alpha$	All	177	0.07	71.0 %
		FSRQ	142	0.09	57.1 %
		BL Lac	29	0.21	51.4 %

TABLE 5 1505 blazars luminosity-Doppler factor.

Fermi name (1)	Class (2)	Redshift (3)	Flux1000 <i>photons/cm²/s</i> (4)	α_{ph} (5)	δ^{L_γ} (6)
4FGLJ0001.5+2113	F	1.106	9.6832E-10	2.6802	10.66
4FGLJ0003.9-1149	B	1.30999	2.8624E-10	2.1267	9.78
4FGLJ0004.0+0840	U	2.057129	2.2296E-10	2.1032	15.62
4FGLJ0004.4-4737	F	0.88	4.8554E-10	2.4152	6.46
4FGLJ0005.9+3824	F	0.229	4.5453E-10	2.6661	1.16
...

that the emission of FDSs is most likely dominated by the discrete flow as indicated by the K-S test result in Table 4. This result suggests that the γ -ray emission from jets occurs not continuously, but acts separately in γ -ray emission, like when a relativistic flow of matter interacts through a shock with interstellar medium, accelerates electrons to relativistic speeds and these electrons scatter soft photons to γ -ray energy in knotty regions, called also ‘hot spots’ or ‘knots’.

In order to investigate the origin of γ -ray photons, we collected the average total flux density at 15 GHz from Lister et al. (2018) and the component flux density at 15 GHz from Lister et al. (2019) for 187 sources, and listed them in Table 6, in which we quote: column (1) name; column (2) classification; column (3) redshift; column (4) the serial number of an individual component; column (5) the 15 GHz component flux density of the corresponding component; column (6) the 15 GHz total flux density of the source; column (7) γ -ray photon spectral index; column (8) integral photon flux from 1 to 100 GeV;

The correlations between L_γ against 15 GHz total luminosity ($L_{15\text{GHz}}^{\text{tot}}$) and component luminosity ($L_{15\text{GHz}}^{\text{com}}$) are shown in Figure 4 and give the following parameterized relation,

$$\log L_\gamma = (0.75 \pm 0.06) \log L_{15\text{GHz}}^{\text{com}} + (21.98 \pm 1.93)$$

with $r = 0.68$ and $p = 3.6 \times 10^{-27}$;

$$\log L_\gamma = (0.97 \pm 0.06) \log L_{15\text{GHz}}^{\text{tot}} + (13.12 \pm 1.96)$$

with $r = 0.78$ and $p = 6.5 \times 10^{-40}$.

These correlations are both good according to their r and p values. The correlation of L_γ against $L_{15\text{GHz}}^{\text{com}}$ indicates that a considerable amount of γ -ray photons originate from ‘hot spots’ or ‘knots’, where particles, accelerated to relativistic speeds, scatter soft photons towards high energies.

4 | CONCLUSIONS

1. We have updated 40 new FDS sources from our 102 non-FDS sources through cross-matching our sample with the 4FGL catalogue;
2. We have found that the non-Fermi detected superluminal sources are γ -ray emitting candidates, this result helps to enlarge the γ -ray AGNs sample;
3. We have proposed that a Doppler factor estimate can be obtained through an empirical formula valid for γ -ray sources, especially for FDSs;
4. We suggest that the γ -ray emission from superluminal sources is discrete and that significant fraction γ -ray emission should arise from ‘knots’ and ‘hot spots’.

TABLE 6 187 FDSs with total and component flux from Lister et al. (2018) and Lister et al. (2019).

Fermi name	Class	Redshift	Component ID	$f_{15\text{GHz}}^{\text{com}}$ <i>mJy</i>	$f_{15\text{GHz}}^{\text{tot}}$ <i>mJy</i>	α_{ph}	Flux1000 <i>photons/cm²/s</i>
(1)	(2)	(3)	(4)	(5)	(6)	(7)	(8)
3FGL J0051.0-0649	F	1.975	1	28	1115.4	2.1047	1.40E-09
3FGL J0102.8+5825	F	0.644	5	154	2530.31	2.0943	6.18E-09
3FGL J0108.7+0134	F	2.107	2	92	2303.69	2.2601	5.27E-09
3FGL J0110.2+6806	B	0.29	1	32	328.8	1.9909	1.92E-09
3FGL J0112.8+3207	F	0.603	3	21	640.44	2.3626	3.04E-09
...

ACKNOWLEDGEMENTS

We would like to thank the nice referee, Prof. Rafanelli, for his corrections and notations made in the manuscript, and his comments and suggestions that let us improve the manuscript. This work was carried out under the auspices of the **National Natural Science Foundation of China** under Contract No. *NSFC 11733001 and NSFC U1531245*, and partially supported by **Natural Science Foundation of Guangdong Province** under Contracts No. *2019B030302001 and 2017A030313011*, support for Astrophysics Key Subjects of Guangdong Province and Guangzhou City, and **Science and Technology Program of Guangzhou** under Contract No. *201707010401*. We also thank the MOJAVE team and Purdue University for the use of the precious kinematic data.

REFERENCES

- Abdo, A. A., Ackermann, M., Agudo, I., et al. 2010, *ApJ*, 716, 30.
 Arshakian, T. G., Torrealba, J., Chavushyan, V. H., et al. 2010, *A&A*, 520, A62.
 Blandford, R. D., Königl, A. 1979, *ApJ*, 1, 232.
 Donato, D., Ghisellini, D., Tagliaferri, G and Fossati, G. 2001, *A&A*, 375, 739.
 Dondi, L & Ghisellini, G. 1995, *MNRAS*, 273, 583.
 Fan, J. H., Xie, G. Z., Li, J. J. 1993, *ApJ*, 415, 113.
 Fan, J. H., Xie, G. Z., Wen, S. L. 1996, *A&AS*, 116, 409.
 Fan, J. H., Yang, J. H., Liu, Y., Zhang, J. Y. 2013a, *RAA*, 13, 259.
 Fan, J. H., Yang, J. H., Zhang, J. Y. et al. 2013b, *PASJ*, 65, 25.
 Fan, J. H., Yang, J. H., Liu, Y., et al. 2016, *ApJS*, 226, 20.
 Fan, J. H., Yang, J. H., Xiao, H. B., Lin, C., et al. 2017, *ApJL*, 835, 38.
Fermi LAT collaboration. 2019, arXiv:1902.10045v2.
 Fossati, G., Maraschi, L., Celotti, A., et al. 1998, *MNRAS*, 299, 433.
 Giovannini, G., Liuzzo, E., Boccardi, B., Giroletti, M. 2014, *IAUS*, 304, 200.
 Giroletti, M., Pavlidou, V., Reimer, A., et al. 2012, *AdSpR*, 49, 1320.
 Hovatta, T., Valtaoja, E., Tornikorski, M., et al. 2009, *A&A*, 496, 527.
 Kovalev, Y. Y., et al. 2009, *ApJ*, 707, 56.
 Liodakis, I., Hovatta, T., Huppenkothen, D., Kiehlmann, S., et al. 2018, *ApJ*, 886, 2.
 Lister, M. L., Cohen, M. H., Homan, D. C., et al. 2009, *AJ*, 138, 1874.

- Lister, M. L., Aller, M. F., Aller, H. D., Homan, D. C., et al. 2013, *AJ*, 146, 120.
 Lister, M. L., Aller, M. F., Aller, H. D., et al. 2018, *ApJ*, 234, 12.
 Lister, M. L., Homan, D. C., Hovatta, T., et al. 2019, *ApJ*, 874, 1.
 Massaro, F., Giroletti, M., Paggi, A., et al. 2013a, *ApJS*, 207, 4.
 Massaro, F., D'Abrusco, R., Giroletti, M., et al. 2013b, *ApJS*, 208, 15.
 Pei, Z. Y., Fan, J. H., et al. 2016, *Ap&SS*, 361, 237.
 Savolainen, T., Homan, D. C., Hovatta, T., et al. 2010, *A&A*, 512A, 24.
 von Montigny, C., Bertsch, D. L., et al. 1995, *ApJ*, 440, 525.
 Xiao, H. B., Fan, J. H., Pei, Z. Y., et al. 2015, *Ap&SS*, 359, 39.
 Xiao, H. B., Fan, J. H., et al. 2019, *SCPMA*, 62, 129811.
 Yang, J. H., Fan, J. H., Liu, Y., Zhang, Y. L., Yang, R. S., Tuo, M. X., et al. 2017, *Ap&SS*, 362, 219.
 Yang, J. H., Fan, J. H., Liu, Y., Zhang, Y. L., Yang, R. S., Tuo, M. X., Nie, J. J. 2018a, *AcASn*, 59, 4.
 Zhang, Y. W & Fan, J. H. 2008, *ChJAA*, 4, 385.
 Zhang, L. X & Fan, J. H. 2018, *Ap&SS*, 363, 142.



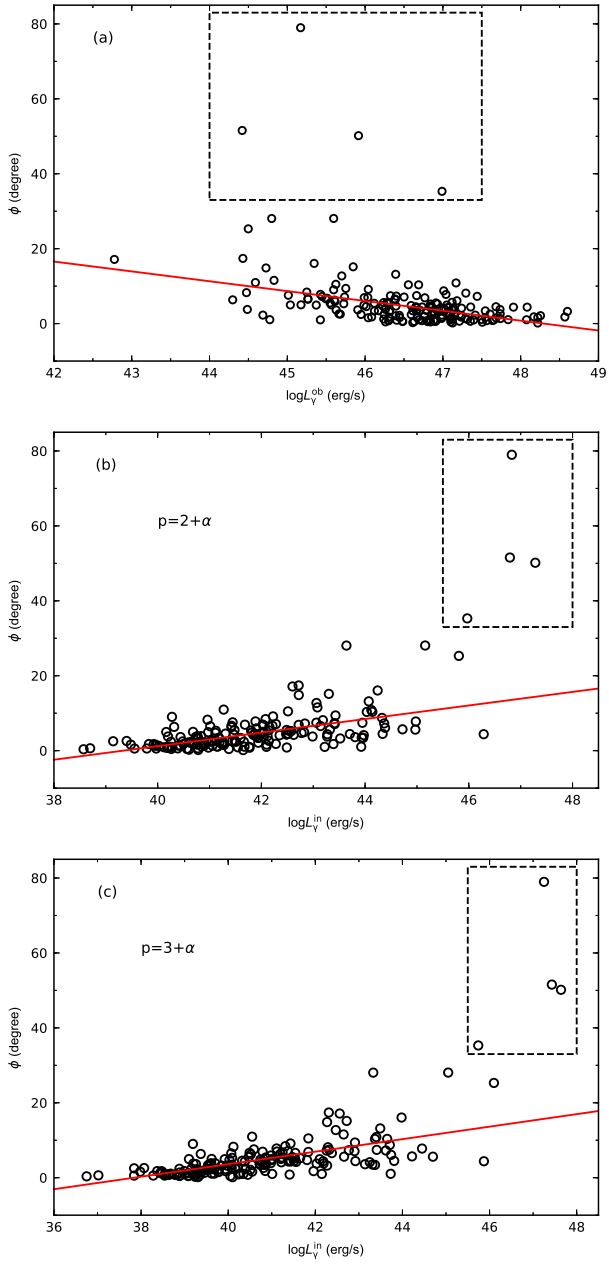


FIGURE 2 Correlation between observed γ -ray luminosity and viewing angle of FDS sources. The solid line shows the best linear fitting result of all the sources (apart from the sources in the dashed rectangle).

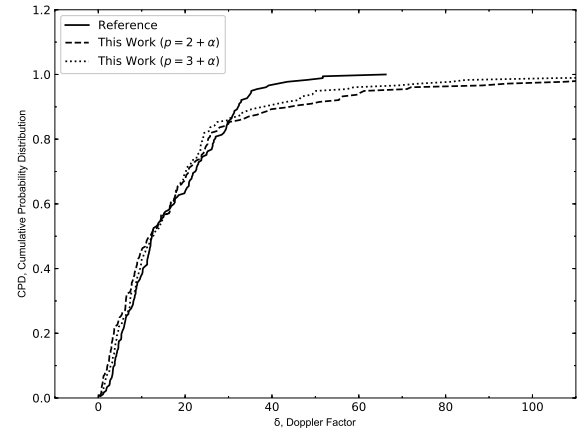


FIGURE 3 K-S test CPD distribution. The solid line for the Doppler factor from literature, while dashed line and dotted line for Doppler factors are calculated in this work with different expression of p .

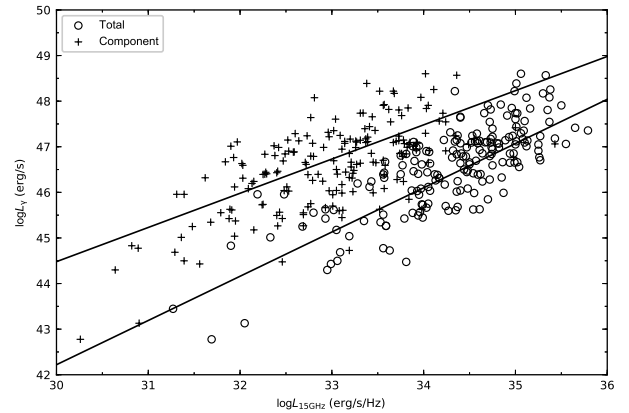


FIGURE 4 Correlation between γ -ray luminosity and radio 15 GHz luminosity, the open dots and the crosses represent the total and the component luminosities respectively.